CASL
A DOE Energy Innovation Hub

CASL-U-2015-0158-000

Transient Methods for Pin-Resolved Whole Core Transport Using the 2D-1D Methodology in MPACT

Ang Zhu, Yunlin Xu, Aaron Graham,
Mitchell Young, and Thomas Downar
University of Michigan

Liangzhi Cao
Xi'an Jiaotong University

April 19, 2015

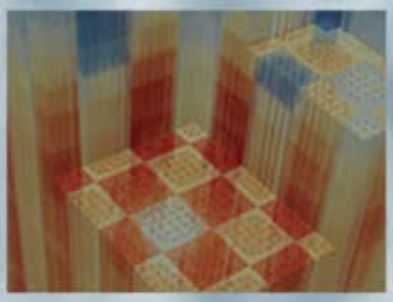

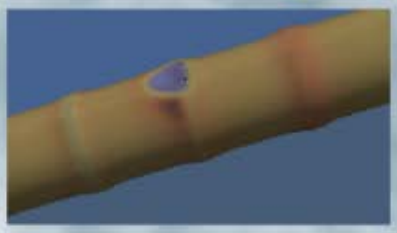

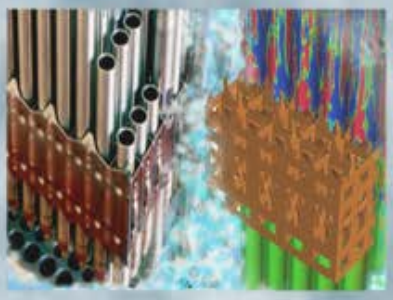

U.S. DEPARTMENT OF ENERGY | Nuclear Energy
CASL-U-2015-0158-000

ANS MC2015 - Joint International Conference on Mathematics and Computation (M&C), Supercomputing in Nuclear Applications (SNA) and the Monte Carlo (MC) Method • Nashville, TN • April 19-23, 2015, on CD-ROM, American Nuclear Society, LaGrange Park, IL (2015)

TRANSIENT METHODS FOR PIN-RESOLVED WHOLE CORE TRANSPORT USING THE 2D-1D METHODOLOGY IN MPACT

Ang Zhu, Yunlin Xu, Aaron Graham, Mitchell Young and Thomas Downar
Department of Nuclear Engineering & Radiological Science
University of Michigan, Ann Arbor, 48105, USA
angzhu@umich.edu; yunlin@umich.edu; aarograh@umich.edu;
youngmit@umich.edu; downar@umich.edu

Liangzhi Cao
School of Nuclear Science and Technology
Xi'an Jiaotong University
caolz@mail.xjtu.edu.cn

ABSTRACT

This paper presents the development and preliminary validation of the transient transport capability within the framework of the pin resolved, 2D-1D method in the core neutronics code MPACT. A description of the transient methodology developed in MPACT is first provided and then two alternative transient CMFD acceleration techniques are described, a one group (1G) and a multigroup (MG) CMFD. Results show that the MG CMFD is more effective for practical transient problems. The NEM nodal transient method is then presented as the 1D axial solver for the 2D-1D method in MPACT. Numerical results are then presented for the 2D TWIGL and 3D SPERT benchmarks. The TWIGL results from MPACT are shown to agree well with the DeCART transport code and other reference solutions. Preliminary results are then shown for the SPERT III test 86 case and the MPACT result is shown to be in reasonable agreement with the experimental data.

Key Words: Transient, MOC, CMFD, TWIGL, SPERT, MPACT

1 INTRODUCTION

MPACT [1, 2] is a three-dimensional (3-D) whole core transport code that is capable of generating sub-pin level power distributions. This is accomplished by obtaining the integral transport solutions to the heterogeneous reactor problem in which the actual pin-resolved geometrical configuration of fuel components such as the pellet and cladding is explicitly retained during the flux solution. The cross section data needed for the neutron transport calculation are obtained directly from a multi-group microscopic cross section library similar to those used in lattice physics codes. Hence MPACT involves neither a priori homogenization nor group condensation for the core spatial solution.

The steady-state integral transport solution is obtained by a means of the method of characteristics (MOC) which employs discrete ray tracing. Since the direct application of MOC to a 3-D core configuration requires considerable amounts of memory and computing time for practical reactor applications, an alternative approximate 3-D solution method was implemented in MPACT based on a 2D-1D approach which employs planar MOC solutions in the framework of the 3-D coarse mesh finite difference (CMFD) formulation [3]. The axial coupling is resolved

by one-dimensional (1-D) diffusion solutions and the planar and axial problems are coupled through the transverse leakage. The use of a lower order 1-D solution in the axial direction is justified by the fact that most heterogeneity in the core occurs in the radial direction rather than the axial. However, it can be easily replaced by a higher order method such as the 1-D SN if greater solution accuracy is needed.

The transient capability was recently designed and implemented in MPACT based on the MOC fine mesh in order to capture the pin-resolved transient power distribution. The first section of this paper describes the transient methodology including the formulation for 2D MOC, 3D CMFD and 1D NEM methods. The second section then presents the numerical results of 2D TWIGL and 3D SPERT benchmarks. The CMFD coarse mesh based whole core adjoint flux calculation capability is also implemented in MPACT and its comparison with MOC based adjoint flux calculation is presented in [4].

2 TRANSIENT METHODOLOGY

In order to determine the time-dependent pin-resolved power distribution, the transient calculation in MPACT is performed based on the MOC flat source region rather than CMFD coarse mesh. For this, the 3D problem domain is first divided into several thick planes and radial flux distribution is solved using the 2D MOC method. The axial coupling is resolved by one-dimensional (1D) diffusion solutions and the planar and axial problems are coupled through the transverse leakage. The use of a lower order 1D solution in the axial direction is justified for most PWR applications since most heterogeneity in the core occurs in the radial direction rather than the axial. A 3D CMFD formulation is developed and used to accelerate the 2D radial and 1D axial solution.

In the following section, the derivation of the MPACT transient solution method begins with the formulation of the multi-group MOC transient fixed source problem (TFSP) which involves the time discretization based on the implicit Euler method and the precursor integration technique. The formulation of the CMFD method is then introduced and two different CMFD iteration schemes were implemented and investigated. The 1G CMFD method updates the transient source based on the current iterate coarse mesh flux and fission source. The 1G CMFD method is shown to require multiple iterations until the transient and fission source are converged. In contrast, the MG CMFD method is more efficient since it adds the transient source into the CMFD matrix and solves the whole matrix in one iteration.

Finally, a two-node NEM kernel is presented in which a second order polynomial is used to approximate the transient source term. Because the same order of polynomial approximation is used for the transient and the steady-state solutions, the existing NEM method was simply modified by adding a transient source into the radial transverse leakage term to solve the transient problem.

2.1 Formulation of 2D MOC Transient Fixed Source Problem

The time dependent form of the planar transport problem which is obtained after integration of the angularly discretized 3-D Boltzmann transport equation can be written as follows for angle m:

$$\frac{1}{v_g}\frac{\partial \varphi_g^m}{\partial t}+\left(\eta_m\frac{\partial \varphi_g^m}{\partial x}+\varepsilon_m\frac{\partial \varphi_g^m}{\partial y}+\Sigma_{tg}\varphi_g^m\right)=\frac{1}{4\pi}\left(\chi_{pg}(1-\beta)\psi+\chi_{dg}S_d+\sum_{g'=1}^{G}\Sigma_{gg'}\phi_{g'}\right)-\frac{\mu_m}{h_z}\left(\varphi_{gT}^m-\varphi_{gB}^m\right) \quad (1)$$

where φ_g^m, ϕ_g, ψ, and S_d are the angular flux of angle *m*, scalar flux, total fission source, and delayed neutron source respectively, which are all axially averaged, whereas φ_{gT}^m and φ_{gB}^m are the angular fluxes at the top and bottom of the plane.

In addition, six more precursor equations are described below:

$$\frac{dC_k}{dt}=\beta_k\psi\ -\lambda_k C_k, k=1,2,...,6 \quad (2)$$

where C_k is the delayed neutron precursor density, and ψ and S_d are the total fission source and the delayed neutron source defined as:

$$\psi\ =\sum_{g=1}^{G}\nu\Sigma_{fg}\phi_g\ , \quad (3)$$

$$S_d=\sum_{k=1}^{K}\lambda_k C_k\ . \quad (4)$$

In the above equations, the ν value is adjusted by the eigenvalue determined in the initial steady-state calculation.

For a given time step size Δt_n at time step *n*, Eq. (1) can be discretized using the implicit Euler method as:

$$\frac{\varphi_g^{m,n}-\varphi_g^{m,n-1}}{v_g^m\Delta t_n}=R_g^{m,n} \quad (5)$$

with $R_g^{m,n}$ denoting all the right hand side terms of Eq. (1) at time step *n*.

Eq. (5) can be rewritten as:

$$\frac{\varphi_g^{m,n}}{v_g^m\Delta t_n}-R_g^{m,n}=\frac{\varphi_g^{m,n-1}}{v_g^m\Delta t_n} \quad (6)$$

The RHS terms of Eq. (6) are all known from the solution of the previous time step and the flux at the current time step is the unknown to be determined. Eq. (6) cannot be solved unless time differencing is performed to the precursor balance equation since the $R_g^{m,n}$ term contains the delayed neutron source term which involves the unknown delayed neutron precursor concentrations at time step *n*. To avoid the time differencing of the precursor equation, one can

eliminate the unknown precursor term C_k^n from $R_g^{m,n}$ by introducing the second order precursor integration technique [5] which is based on the second order variation of the fission source during the current time step. As a result, the delayed neutron source can be expressed as:

$$S_d^n = \sum_{k=1}^{K} \lambda_k C_k^{n-1} e^{-\lambda_k \Delta t_n} + \sum_{l=n-2}^{n} \sum_{k=1}^{K} \beta_k \Omega_k^l \psi^l \equiv \tilde{S}_d^{n-1} + \omega^n \psi^n \tag{7}$$

where

$$\Omega_k^{n-2} = \frac{1}{\lambda_k \Delta t_{n-1}(\gamma+1)} \left(\frac{2(1-\kappa_k)}{\lambda_k \Delta_{t_{n-1}}} - \gamma(\kappa_k + 1) \right),$$

$$\Omega_k^{n-1} = \frac{1}{\lambda_k \Delta t_{n-1}} \left(\kappa_k + 1 + \frac{1-\kappa_k}{\gamma} \left(1 - \frac{2}{\lambda_k \Delta t_{n-1}} \right) \right) - \kappa_k ,$$

$$\Omega_k^{n} = 1 - \frac{2}{(\gamma+1)\lambda_k \Delta t_{n-1}} + \frac{1-\kappa_k}{\gamma(\gamma+1)\lambda_k \Delta t_{n-1}} \left(\frac{2}{\lambda_k \Delta t_{n-1}} - 1 \right),$$

$$\tilde{S}_d^{n-1} = \sum_{k=1}^{K} \kappa_k \lambda_k C_k^{n-1} + \sum_{l=n-2}^{n-1} \sum_{k=1}^{K} \beta_k \Omega_k^l \psi^l \tag{8}$$

and

$$\omega^n = \sum_{k=1}^{K} \beta_k \Omega_k^n . \tag{9}$$

with $\kappa_k = e^{-\lambda_k \Delta t_n}$ and $\gamma = \dfrac{\Delta t_n}{\Delta t_{n-1}}$.

By inserting the delayed neutron source terms determined by the previous time step values, Eq. (8), into Eq. (6) and expressing all the terms of $R_g^{m,n}$ explicitly, one can obtain the following transient fixed source problem:

$$\begin{aligned} &\left(\eta_m \frac{\partial \varphi_g^{m,n}}{\partial x} + \varepsilon_m \frac{\partial \varphi_g^{m,n}}{\partial y} \right) + \left(\Sigma_{tg} + \frac{1}{\theta v_g \Delta t_n} \right) \varphi_g^{m,n} \\ &\qquad = \frac{1}{4\pi} \left(\left(\chi_{pg}(1-\beta) + \chi_{dg} \omega \right) \psi^n + \sum_{g'=1}^{G} \Sigma_{gg'} \phi_{g'}^n \right) \\ &\qquad - \frac{\mu_m}{h_z} \left(\varphi_{gT}^m - \varphi_{gB}^m \right) + \frac{\varphi_g^{m,n-1}}{v_g \Delta t_n} + \frac{1}{4\pi} \chi_{dg} \tilde{S}_d^{n-1} \end{aligned} \tag{10}$$

In principle, Eq. (10) can be solved by MOC as long as the RHS is exactly known for each flat source region. However, there are several practical difficulties in solving Eq. (10). First, the total cross section is augmented by the $1/v\Delta t$ term. This augmentation changes the ray attenuation characteristics in the MOC solution since all the exponential terms have to be evaluated with the augmented cross section. Secondly, since the angular flux of the previous step appears on the RHS, all the angular flux should be stored at every flat source region, which would cause a significant increase in the memory.

In order to avoid these problems, the $1/v\Delta t$ term of the current time step is first moved to the RHS so that the left hand side becomes identical to the steady-state form. The angular dependence of the $1/v\Delta t$ term is then neglected by treating this term as isotropic. This approximation would have negligible impact since the isotropy assumption is applied to the difference term, rather than the angular flux itself. Furthermore the angular dependence of the residual term is neglected. Eq. (10) now becomes

$$\begin{aligned}\left(\eta_m \frac{\partial \varphi_g^{m,n}}{\partial x} + \varepsilon_m \frac{\partial \varphi_g^{m,n}}{\partial y}\right) + \Sigma_{tg}\varphi_g^{m,n} &= \frac{1}{4\pi}\left(\left(\chi_{pg}(1-\beta)+\chi_{dg}\omega\right)\psi^n + \sum_{g'=1}^{G}\Sigma_{gg'}\phi_{g'}^n\right) \\ &- \frac{\mu_m}{h_z}\left(\varphi_{gT}^m - \varphi_{gB}^m\right) + \frac{1}{4\pi}\left(\chi_{dg}\tilde{S}_d^{n-1} - \frac{\phi_g^n - \phi_g^{n-1}}{v_g \Delta t_n}\right)\end{aligned} \tag{11}$$

Once the delayed neutron source and the residual terms are given for each flat source region, Eq. (11) can be solved using the steady-state MOC solver with only a few additions of source terms. The final equation becomes:

$$\begin{aligned}&\left(\eta_m \frac{\partial \varphi_g^{m,n}}{\partial x} + \varepsilon_m \frac{\partial \varphi_g^{m,n}}{\partial y}\right) + \Sigma_{tg}\varphi_g^{m,n} \\ &= \frac{1}{4\pi}\left(\chi_g \psi^n + \sum_{g'=1}^{G}\Sigma_{gg'}\phi_{g'}^n\right) - \frac{\mu_m}{h_z}\left(\varphi_{gT}^m - \varphi_{gB}^m\right) + \frac{1}{4\pi} S_{tr}^{g,n},\end{aligned} \tag{12}$$

Since $\chi_g = \chi_{pg}(1-\beta) + \chi_{dg}\beta$, the transient source in Eq. (12) can be defined and simplified as:

$$S_{tr}^{g,n} = \chi_{dg}(\omega-\beta)\psi^n + \chi_{dg}\tilde{S}_d^{n-1} - \frac{\phi_g^n - \phi_g^{n-1}}{v_g \Delta t_n} \tag{13}$$

In order to work with CMFD acceleration and nodal NEM method, the transient source is rearranged as below:

$$\begin{aligned}S_{tr}^{g,n} &= -\frac{\varphi_g^n}{\theta v_g \Delta t_n} + \chi_{dg}(\omega-\beta)\psi^n + \chi_{dg}\tilde{S}_d^{n-1} + \frac{\phi_g^{n-1}}{v_g \Delta t_n} \\ &= A\phi_g^n + B\psi^n + C\end{aligned} \tag{14}$$

where A and B are flux and fission source-dependent terms, while C is a constant term:

$$A = -\frac{1}{v_g \Delta t_n}$$
$$B = \chi_{dg}(\omega - \beta) \tag{15}$$
$$C = \chi_{dg}\tilde{S}_d^{n-1} + \frac{\phi_g^{n-1}}{v_g \Delta t_n}$$

2.2 Coarse Mesh Finite Difference (CMFD) acceleration

Two types of CMFD acceleration methods were developed in MPACT for the transient calculation, a one-group (1G) CMFD and a multi-group (MG) CMFD. The 1G CMFD solves the CMFD equation group by group and requires multiple iterations to converge the final solution, especially for transient problems with a large power change. The MG CMFD formulates one single matrix for the whole 3D CMFD problem and uses PETSc [6] to solve the $Ax=b$ problem. The MG CMFD is recommended since it formulates the entire CMFD matrix and the transient fixed source problem is solved in one iteration which runs much faster than 1G CMFD for all problems analyzed here.

2.2.1 1G CMFD Formulation

Similar to the MOC equation, the CMFD based neutron balance equation can be easily formulated by adding a transient source term. The transient source in the equation is CMFD coarse mesh based and is homogenized based on the flat source fine mesh.

$$\sum_{u=x,y,z} \frac{1}{h_u^m}\left(J_{gu}^{m+} - J_{gu}^{m-}\right) + \Sigma_{rg}^m \phi_g^{m,n} = \chi_g \psi^m + \sum_{\substack{g'=1 \\ g' \neq g}}^{G} \Sigma_{gg'}^m \phi_{g'}^{m,n} + S_{tr}^{m,n} \tag{16}$$

Instead of homogenizing the fine mesh transient source term, the transient source coefficients A, B and C are homogenized by the following equation:

$$A_g^m = \frac{\sum_{i=1}^{I^m} A_g^{m,i} \phi_g^{m,i} V^{m,i}}{\sum_{i=1}^{I^m} \phi_g^{m,i} V^{m,i}}, B^m = \frac{\sum_{i=1}^{I^m} B^{m,i} \psi^{m,i} V^{m,i}}{\sum_{i=1}^{I^m} \psi^{m,i} V^{m,i}}, C^m = \frac{\sum_{i=1}^{I^m} C^{m,i} V^{m,i}}{\sum_{i=1}^{I^m} V^{m,i}} \tag{17}$$

As a result, the CMFD transient source can be updated by the new CMFD flux and fission source:

$$S_{tr,g}^{m,n} = A_g^m \phi_g^n + B^m \psi^n + C^m \tag{18}$$

The 1G CMFD acceleration technique is similar to the traditional steady-state CMFD acceleration technique, however the 1G transient CMFD does not need to update the eigenvalue for each CMFD iteration. In each CMFD iteration, the transient source is updated using the new calculated CMFD flux and fission source using Eq. (18) and added to the right hand side as a source term. The steady-state CMFD then is used to calculate the transient CMFD fixed source problem.

The flow chart is shown in Figure 1. One disadvantage of the 1G method is that it needs multiple CMFD iterations to converge before each MOC solve and the number of iterations can

be very large for transient problems with large power changes since the right hand side (fission source and transient source) can change considerably during an each transient step.

2.2.2 MG CMFD Formulation

In order to improve the slow convergence of the 1G CMFD, a MG CMFD method was developed. The basic idea of this method is to add a transient source coefficient into the CMFD matrix and solve the whole matrix in one iteration. Unlike the steady-state eigenvalue calculation, the transient calculation does not need to update the eigenvalue during a transient step. As a result, the CMFD flux dependent source (including the transient source and fission source) on the right hand side in the transient matrix can be moved to the left hand side and the matrix can then be solved in one iteration.

The following notations are used to summarize the matrix operations:

- Removal term: $\mathbf{M} = -\nabla \mathbf{D} \nabla + \mathbf{\Sigma_t}$
- Scattering: $\mathbf{S} = \mathbf{\Sigma_S}$
- Fission source: $\mathbf{F} = \chi \upsilon \mathbf{\Sigma_f} / k_{eff}$
- The transient source is defined in equation Eq. (14) : $\mathbf{S}_{tr} = \mathbf{A}\phi + \mathbf{BF}\phi + \mathbf{C}$
- Scalar flux vector: ϕ

The neutron balance equation for the MG CMFD is:

$$(\mathbf{M} - \mathbf{S})\phi = \mathbf{F}\phi + \mathbf{A}\phi + \mathbf{BF}\phi + \mathbf{C} \tag{19}$$

Moving the flux dependent term from right hand side to the left hand side, this becomes:

$$(\mathbf{M} - \mathbf{S} - \mathbf{F} - \mathbf{A} - \mathbf{BF})\phi = \mathbf{C} \tag{20}$$

The above equation is a standard linear system and the unknown flux can be solved in one iteration using any matrix inversion method. Another advantage of this method is the unknown flux calculated by the MG CMFD is fully converged while the 1G CMFD only converges to the convergence criteria specified by user input, which is typically set to 1E-4 in MPACT.

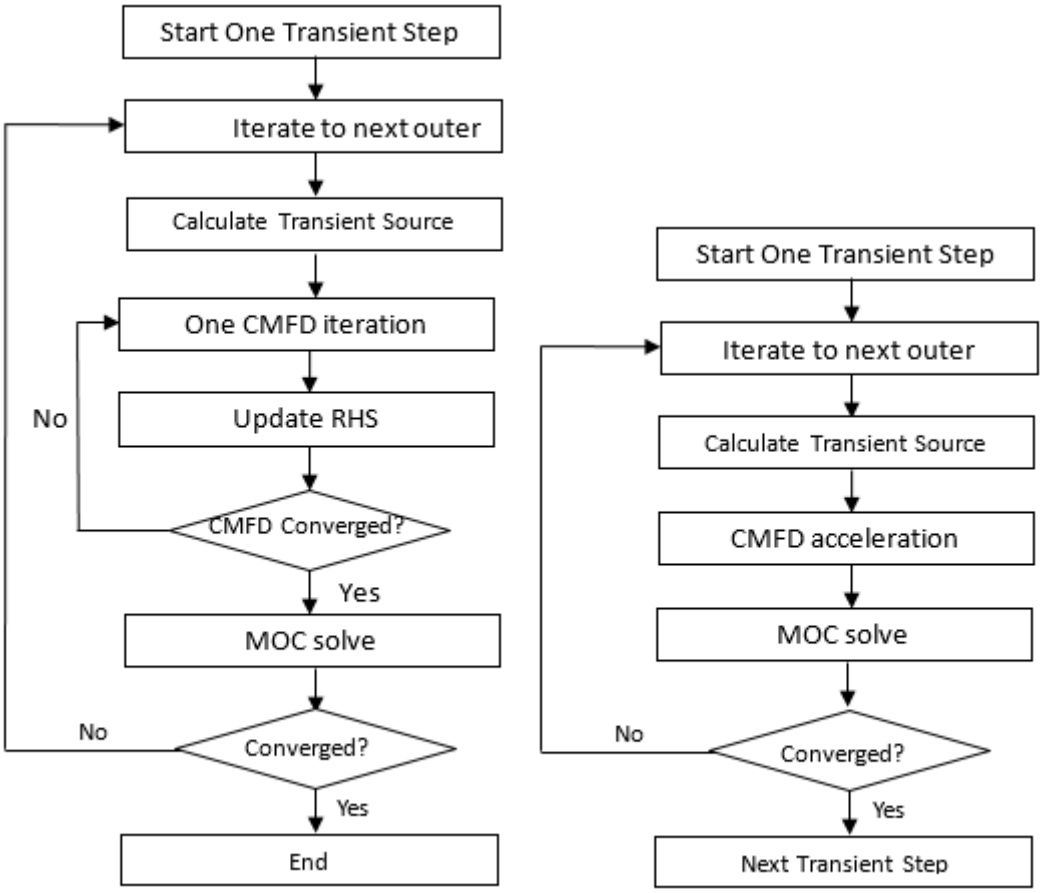

Figure 1 Flow chart for 1G (left) and MG (right) CMFD

2.3 Transient Two-Node NEM Formulation

The TFSP of Eq. (12) contains the axial net current which is to be determined by the Nodal Expansion Method (NEM). Specifically, the net current is solved for the given incoming current boundary condition specified at the top and bottom surfaces of the node. To derive an expression that represents the net current in terms of the incoming partial current and the node average flux, the one-dimensional, one-group continuous form of the TFSP can be written as follows:

$$-D\frac{d^2\phi_g^n(z)}{dz^2}+\Sigma_{rg}\phi_g^n(z)=-L_R^n(z)+\chi_g\psi^n(z)+\sum_{\substack{g'=1\\g'\neq g}}^{G}\Sigma_{gg'}^m\phi_{g'}^n(z)+S_{tr}^{g,n}(z) \tag{21}$$

where the radial transverse leakage is defined as:

$$L_R^n(z)=\sum_{u=x,y}\frac{1}{h_u}\left(J_{gu}^{n+}(z)-J_{gu}^{n-}(z)\right) \tag{22}$$

and the transient source is defined as:

$$S_{tr}^{n}(z) = \left(\chi_{dg}(\omega^{n} - \beta^{n})\right)\psi^{n}(z) + \chi_{dg}\tilde{S}_{d}^{n-1}(z) - \frac{\phi_{g}^{n}(z) - \phi_{g}^{n-1}(z)}{v_{g}^{m}\Delta t_{n}} \tag{23}$$

It is assumed here that the fission source and fluxes of the other groups as well as the last three terms originating from the previous time step are all known and the incoming currents are specified at the top and bottom surfaces of the node.

In principle, the steady-state NEM equation can be solved by using a fourth order polynomial expansion for the flux, a second order polynomial for the transverse leakage term and a fourth order polynomial expansion for the fissions source term. For brevity the detailed expressions for the coefficients are not given here and can be found in [5].

A second order polynomial expansion is used to approximate the transient fixed source term:

$$hS_{tr}^{n}(\xi) = \sum_{k=0}^{2} s_{tr,k} P_{k}(\xi) \tag{24}$$

where $P_0(\xi) = 1,\ P_1(\xi) = \xi,\ P_2(\xi) = \frac{1}{2}(3\xi^2 - 1)$ are the Legendre polynomials.

The transient source moments are calculated as follows:

$$\begin{aligned}
s_{tr,0} &= h^{c} S_{tr}^{c} \\
s_{tr,1} &= G^{-1}\left(h^{c}\right)^{2}\left[(S_{tr}^{r} - S_{tr}^{c})(h^{c} + 2h^{l})(h^{c} + h^{l}) - (S_{tr}^{l} - S_{tr}^{c})(h^{c} + 2h^{r})(h^{c} + h^{r})\right] \\
s_{tr,2} &= G^{-1}\left(h^{c}\right)^{3}\left[(S_{tr}^{r} - S_{tr}^{c})(h^{c} + h^{l}) + (S_{tr}^{l} - S_{tr}^{c})(h^{c} + h^{r})\right] \\
G &= 2(h^{c} + h^{l})(h^{c} + h^{r})(h^{c} + h^{l} + h^{r})
\end{aligned} \tag{25}$$

Where $s_{tr,0}$, $s_{tr,1}$ and $s_{tr,2}$ are 0th, 1st, and 2nd transient source moments, S_{tr}^{n} is the average transient source in the node and h is the length of the node. The superscript *c*, *l* and *r* denote the current, left and right node, respectively.

Due to the use of a second order approximation of the transient source, which is identical to the treatment of the radial transverse leakage term, the NEM solver used for the steady-state calculation can be used almost directly by adding the transient source term into the transverse leakage term.

2.4 Iteration Strategy

The overall iteration scheme of the MPACT transient algorithm is shown in Figure 2. The 2D MOC transport problem or the 2D MOC/1D NEM problem are iteratively solved with 2D or 3D CMFD acceleration until the convergence criteria are satisfied.

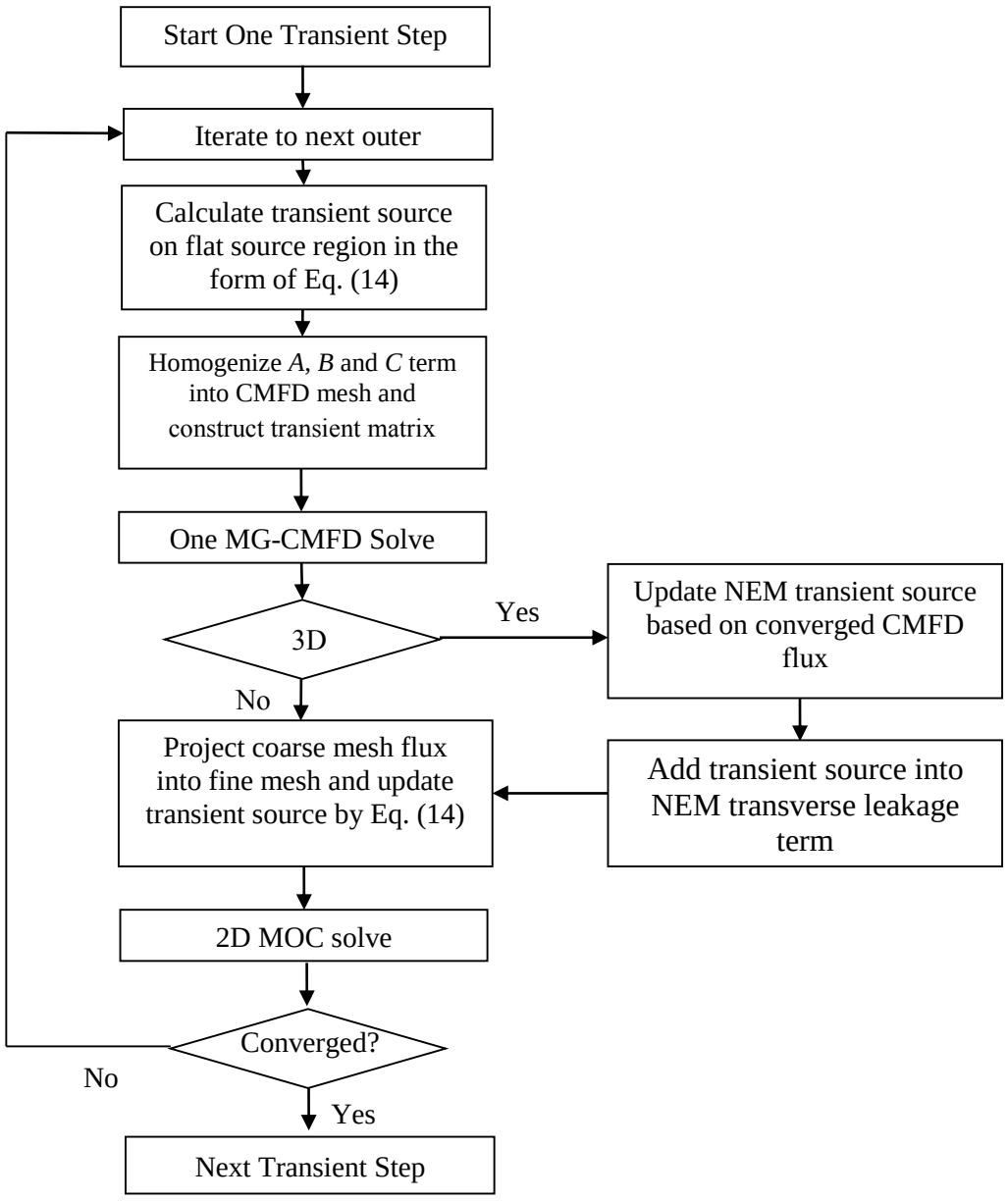

Figure 2 MPACT transient iteration scheme

3 NUMERICAL RESULTS

3.1 TWIGL Benchmark Problem

The TWIGL benchmark problem [7] was used to test and verify the transient solution methodology in MPACT. TWIGL is a simple quarter-symmetric reactor with three different homogeneous regions (see Figure 3). The initial state of the reactor has regions 1, 2 and 3 composed of materials 1, 2, and 3, respectively. Following the initial state, the material composition of region 1 is perturbed as described in Table III.

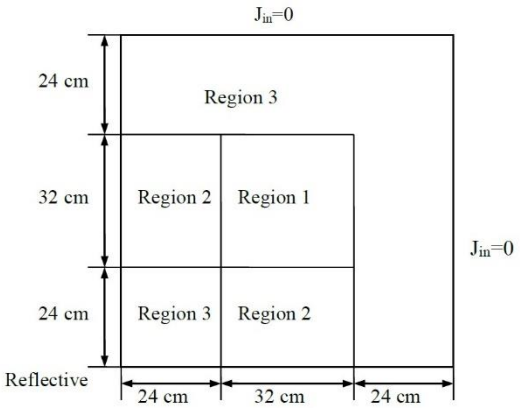

Figure 3 Geometry for the TWIGL 2G Benchmark Problem (adopted from [8])

Since TWIGL was originally formulated as a benchmark for diffusion-based codes, equivalent transport data have been calculated and are shown in Table I below. All the decay neutron data is tabulated in Table I and Table II.

Table I Material compositions

Material	Group	Σ_a	$\nu\Sigma_f$	$\Sigma_{s,gg}$	$\kappa\Sigma_f$	χ
1	1	1.00000E-02	7.00000-03	2.18095E-01	1.12000E-13	1.0
	2	1.50000E-01	2.00000E-01	6.83333E-01	3.20000E-12	0.0
2	1	1.00000E-02	7.00000E-03	2.18095E-01	1.12000E-13	1.0
	2	1.50000E-01	2.00000E-01	6.83333E-01	3.20000E-12	0.0
3	1	8.00000E-03	3.00000E-03	2.38410E-01	4.80000E-14	1.0
	2	5.00000E-02	6.00000E-02	6.16667E-01	9.60000E-13	0.0
4	1	1.00000E-02	7.00000E-03	2.18095E-01	1.12000E-13	1.0
	2	1.46500E-01	2.00000E-01	6.83333E-01	3.20000E-12	0.0
5	1	1.00000E-02	7.00000E-03	2.18095E-01	1.12000E-13	1.0
	2	1.51750E-01	2.00000E-01	6.83333E-01	3.20000E-12	0.0
6	1	1.00000E-02	7.00000E-03	2.18095E-01	1.12000E-13	1.0
	2	1.53500E-01	2.00000E-01	6.83333E-01	3.20000E-12	0.0

Table II Composition-independent quantities

Delayed precursor yield (β)	0.0064
Delayed precursor decay (λ, sec-1)	0.08
Neutron velocity (cm/s)	1.0E+07, 1.0E+05
Delayed neutron spectrum (χ_d)	1.0, 0.0
Down scatter Cross Section (cm-1)	0.01

Table III Transient perturbations applied to Region 1

Time (sec)	Perturbation
0.0 -> 0.2	Linear change: material 1 to material 4

0.2	Step change: material 1 to material 5
0.2 -> 0.4	Linear change: material 1 to material 6
0.4	Step change: material 1 to material 1

The TWIGL benchmark was run using a range of fixed time steps and compared to the solution obtained by the DeCART code [8], which used the theta method with the addition of adaptive time stepping. The MPACT discretization used a ray spacing of 0.03 cm, 16 azimuthal and 3 polar angles with a Chebyshev-Yamamoto quadrature.

As shown in Table IV there is good agreement between the steady-state k_{eff} of MPACT and DeCART. Figure 4 shows the total core power history throughout the course of the transient, and Table V provides a comparison of several power metrics, including peak, asymptotic and integral power. For a 2.5 ms time step, the MPACT simulation ran in approximately 24 minutes using 16 cores with 2.4GHz AMD processors.

Table IV Initial k-eff for TWIGL

Codes	k-eff
DeCART	0.91605
MPACT	0.91601

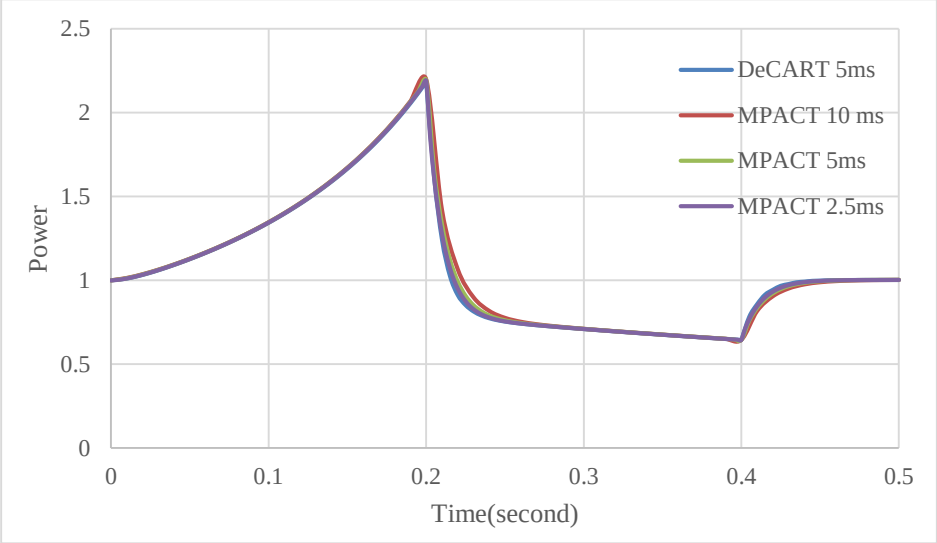

Figure 4 TWIGL core power history

As indicated, the codes agree very well during the ramp reactivity insertion from 0.0 to 0.2 seconds, and all temporal discretizations were capable of accurately calculating the increase in power and the peak power. Minor discrepancies are noticeable immediately following the step insertions, where finer time steps are required to resolve the large increase in the magnitude of the flux time derivative. The peak and asymptotic powers agree well and are within a percent error, with the integral power being the most affected with about a 1% difference from the DeCART result for the 10 ms MPACT result. Table VI shows the region-wise averaged

normalized pin power. For a time step of 2.5 ms, MPACT agrees well with DeCART result with an error of less than 0.02%.

Table V Power metric comparisons.

	$\Delta_t = 10$ ms	$\Delta_t = 5$ ms	$\Delta_t = 2.5$ ms	Ref(DeCART)
Peak Power	2.198	2.192	2.189	2.183
Asymptotic Power	1.003	1.003	1.003	1.002
Integral Power	0.541	0.538	0.536	0.535

Table VI Region wise pin power comparison

Time(second)	Region	MPACT	DeCART	Error
0.0	1	1.5699	1.5698	-0.01%
	2	1.9935	1.9934	0.00%
	3	0.4506	0.4507	0.02%
0.1	1	1.5937	1.5936	-0.01%
	2	1.9815	1.9815	0.00%
	3	0.4491	0.4491	0.00%
0.2	1	1.6183	1.6182	-0.01%
	2	1.9690	1.9689	0.00%
	3	0.4475	0.4476	0.02%
0.3	1	1.5363	1.5362	-0.01%
	2	2.0109	2.0108	0.00%
	3	0.4526	0.4527	0.02%
0.4	1	1.5255	1.5255	0.00%
	2	2.0165	2.0164	0.00%
	3	0.4533	0.4533	0.00%
0.5	1	1.5699	1.5698	-0.01%
	2	1.9935	1.9934	0.00%
	3	0.4506	0.4507	0.02%

3.2 SPERT benchmark result

One of the most frequently used experiments for transient validation has been the Special Power Excursion Reactor Test (SPERT) project which was established as part of the U. S. Atomic Energy Commission's reactor safety program in 1954. Among the several SPERT core designs, the E-Core consisting of 60 assemblies was used to perform reactivity insertion accident (RIA) experiments, and the data measured during those experiments was used here to validate the neutronics performance of the MPACT code transient conditions. The core geometry is shown in Figure 5 and the SPERT III E-core Reactor Component Design Data from [9] and [10] are documented in [11]. A comparison of the steady-state MPACT solution for the Hot Zero Power (HZP) and Cold Zero power (CZP) critical core configuration of the SPERT E-Core are compared to KENO in Table VII. As indicated both MPACT and KENO are within a few hundred pcm of criticality which provides confidence in the MPACT model of the SPERT E-

Core. The detailed power distribution comparisons of MPACT and KENO for the critical cores are provided in [11].

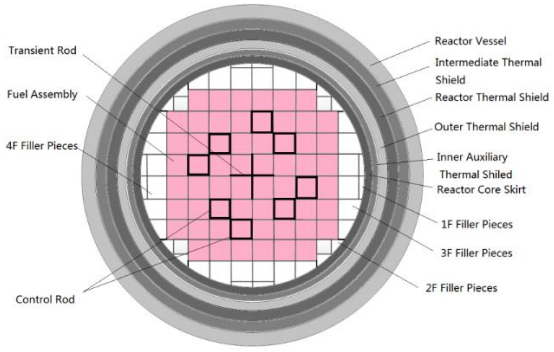

Figure 5 SPERT III E-core cross-section

Table VII Comparison of Eigenvalues for Critical Core Configurations [11]

Case	Temp. (F)	C.R. Pos.(cm)	MPACT	KENO-CE
CZP	70	36.957	0.99613	1.00028
HZP	550	71.755	1.00023	1.00356

The SPERT III E-Core control rod ejection tests consisted of a sequence of CZP, HZP, and HFP tests with various transient rod insertion depths. For brevity, only the HFP test 86 will be used here to demonstrate the preliminary validation of MPACT. Transient test 86 is a hot full power transient where the initial core inlet temperature are at 502 ^{o}F ± 4 ^{o}F. The system is also pressurized such that the initial thermal hydraulic condition is within typical PWR operating conditions. In addition, the initial reactor power is approximately 19 ± 1 MW. The withdrawn transient rod worth is \$1.17 ± 0.05, which is simulated by linearly changing the transient rod composition in the withdrawn part of the rod.

The SPERT cases were run in MPACT using TCP0 scattering with 0.05 ray spacing and the Chebyshev-Gauss quadrature set was used with 4 azimuthal and 1 polar angles. The multi-group NEM kernel was used to perform the axial solution with 20 axial layers. The cross sections for MPACT were provided from a 56−group AMPX library generated at ORNL by CASL[12]. The thermal-hydraulics feedback for the transient solution was provided by an internal thermal-hydraulics module in MPACT which solves transient mass and energy equations. Future work will include the coupling of the MPACT transient solver to the subchannel thermal-hydrualics code COBRA-TF.

The execution time for Test 86 with 2880 cores on the Titan compute cluster at ORNL was approximately 2 hours. The preliminary result of the power calculated by MPACT is shown in Figure 6 and as indicated there is reasonable agreement with the measurement data. However there are some noticeable discrepancies, especially at the start of the pulse. This bias is primarily due to the simplified transient rod movement mechanism currently used in MPACT, where the axial effect of the transient rod worth and transient rod acceleration mechanism are not

considered. Also, a coarse quadrature set and a first order time discretization was used in the preliminary calculations. A finer quadrature set with 16 azimuthal angles and 4 polar angles will be used for subsequent validation calculations.

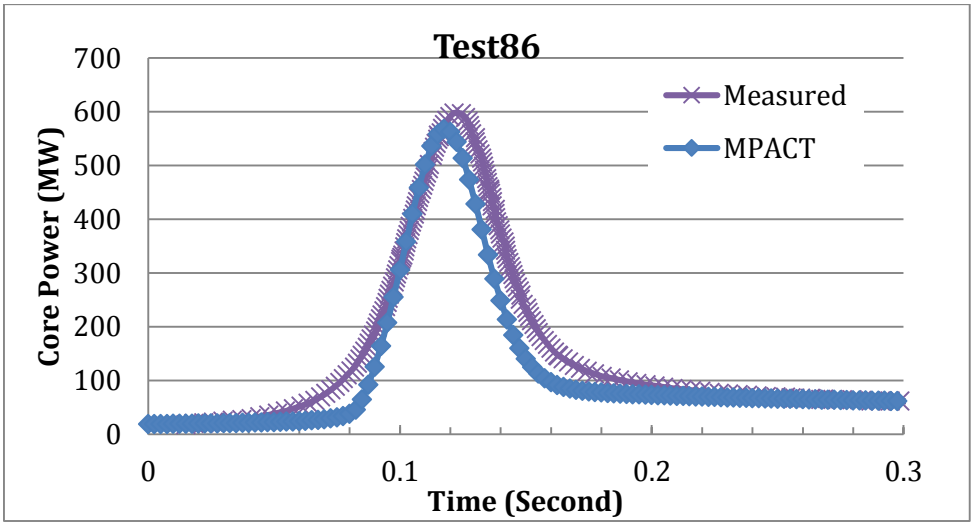

Figure 6 Test 86 core power history

4 SUMMARY AND CONCLUSIONS

The objective of this paper was to present the development and preliminary validation of the transient capability of the MPACT code. The transient formulation for the pin-resolved 2D-1D method was first presented and then two alternative transient CMFD acceleration techniques were discussed, a 1-Group (1G) CMFD and Multigroup (MG) CMFD. Results showed that the MG CMFD was more effective since it solves the entire CMFD matrix in one iteration and dramatically accelerates the transient solution. The NEM nodal transient method was then presented as the 1D axial solver for the 2D-1D method. Numerical results were then presented for the 2D TWIGL and 3D SPERT benchmarks. The TWIGL 2G benchmark result of MPACT were shown to agree very well with the DeCART reference solution. The preliminary results for the SPERT III test 86 cases were then provided and the preliminary results of MPACT were in reasonable agreement with the experimental data.

Work is continuing on transient methods development in MPACT. This will include the implementation of improved rod ejection logic in MPACT, a higher order time discretization method, an axial SPN transport kernel will be implemented in MPACT, and the transient neutronics will be coupled to the transient TH solver in COBRA-TH. A complete set of SPERT experiments will then be performed to validate the MPACT transient capability with the coupled codes MPACT/COBRA-TF. The final goal is to apply MPACT to the analysis of an RIA "challenge problem" as part of the CASL core simulator VERA-CS.

5 ACKNOWLEDGMENTS

This research was supported by the Consortium for Advanced Simulation of Light Water Reactors (www.casl.gov), an Energy Innovation Hub (http://www.energy.gov/hubs) for Modeling and Simulation of Nuclear Reactors under U.S. Department of Energy Contract No. DE-AC05-00OR22725.

6 REFERENCES

1. MPACT Team, MPACT Theory Manual, Version 1.0 , University of Michigan, Ann Arbor, MI, October, 2013.
2. B. Kochunas, et al, "Overview of Development and Design of MPACT: Michigan Parallel Characteristics Transport Code", Proc. Int. Conf. Mathematics and Computational Methods Applied to Nuclear Science & Engineering (M&C 2013), American Nuclear Society, Sun Valley, ID, USA, May 5-9, [CD-ROM] (2013)
3. B. Kelly and E. Larsen, "2D/1D Approximations to the 3D Neutron Transport Equation: Theory," International Conference on Mathematics and Computational Methods Applied to Nuclear Science & Engineering (M&C 2013) Sun Valley, Idaho, USA, May 5-9, 2013
4. A. Zhu, et al, "The Implementation and Analysis of the MOC and CMFD Adjoint Capabilities in the 2D-1D Code MPACT", Joint International Conference on Mathematics and Computation (M&C), Supercomputing in Nuclear Applications (SNA) and the Monte Carlo (MC) Method (M&C 2015), American Nuclear Society, Nashville, TN, USA, April 19-23, [CD-ROM] (2015)
5. T. Downar, Y. Xu, V. Seker, PARCS v3.0 U.S. NRC Core Neutronics Simulator User/Theory Manual, Department of Nuclear Engineering and Radiological Sciences University of Michigan, Ann Arbor, MI, September 2009.
6. S. Balay, et al. PETSc Users Manual Revision 3.4[J]. 2013.
7. "The Numerical Nuclear Reactor for High Fidelity Integrated Simulation of Neutronic, Thermal-Hydraulic and Thermo-Mechanical Phenomena, Final Report," International Nuclear Energy Research Initiative, Project Number 2002-010-K (2005).
8. J. Cho, et al. Transient capability of the DeCART code[R]. Korea Atomic Energy Research Institute, Taejon (Korea, Republic of), 2005.
9. J. Durgone, SPERT III Reactor Facility: E-CORE Revision, AEC Research and Development Report IDO-17036, November 1965.
10. M. Jessee, M.D. DeHART, TRITON: A Multipurpose Transport, Depletion, and Sensitivity and Uncertainty Analysis Module, T1.3.11, Version 6.1, Sect T1, Oak Ridge National Laboratory, Reactor and Nuclear Systems Division, June 2011.
11. L. Cao, et al., "Neutronics Modeling of the SPERT III E-Core Critical Experiments with MPACT and KENO," *Annals of Nuclear Energy*, **80** (2015) 207–218
12. CASL(Consortium for Advanced Simulation of Light Water Reactors), http://www.casl.gov/